JOURNAL OF Materials CHEMISTRY

Synthesis of NbS_2 nanoparticles with (nested) fullerene-like structure (*IF*)

Christoph Schuffenhauer, Ronit Popovitz-Biro and Reshef Tenne*

Department of Materials and Interfaces, Weizmann Institute of Science, Rehovot 76100, Israel. E-mail: Reshef.Tenne@weizmann.ac.il

Received 9th November 2001, Accepted 25th January 2002
First published as an Advance Article on the web 26th March 2002

NbS_2 nanoparticles with a closed cage structure (inorganic fullerene-like phase—*IF*) were synthesized by reaction between $NbCl_5$ vapor and H_2S gas in a reducing atmosphere at 400 °C, and subsequent annealing under a H_2S/H_2 atmosphere at 550 °C. Following the synthesis, the nanoparticles were found to have a large excess of Nb; they were agglomerated; highly dislocated and enfolded by amorphous material. After annealing, most of the amorphous material crystallized into closed NbS_2 shells, and the nanoparticles appeared to be much more faceted. Transmission electron microscopy revealed that the interlayer spacing (*c*/*n*) of the annealed particles had decreased. They were also agglomerated, being connected to neighboring nanoparticles through their outer NbS_2 layers after annealing. In related experiments Nb_2O_3 nanofibers, which organize into a nanoflower superstructure, and also NbS_2 nanofibers were synthesized under somewhat different growth conditions.

Introduction

Nanoparticles of (2-D) layered compounds have been shown to be unstable against folding and they form structures analogous to (nested) carbon fullerenes and nanotubes, which have been hailed as inorganic fullerene-like materials (*IF*). Early experiments with tungsten and molybdenum disulfides[1,2] have been extended to BN,[3] and numerous other layered compounds. Various methods were proposed for the synthesis of such phases. Essentially these methods involve arrested growth of the crystallites. This growth mode implies that energy minimization occurs within the nanoparticle itself without energy or material transfer between the nanoparticles. Consequently the most stable closed cage nanostructures (*IF*) are obtained in such processes. Recently, a number of reports describing the growth of NbS_2 and TaS_2 nanotubes and fullerene-like structures have appeared. Thus, Nb doped WS_2 nanotubes were obtained by first depositing Nb_2O_5 onto pre-prepared $W_{18}O_{49}$ nanowhiskers, with subsequent annealing in H_2S gas at elevated temperatures.[4] MS_2 (M = Nb, Ta) nanotubes were obtained *via* the reduction of the respective MS_3 at 1000 °C.[5] Nested fullerene-like structures (onions) of NbS_2 were obtained by annealing Nb_2O_5 nanoparticles in H_2S in the presence of active carbon.[6] NbS_2 nanotubes were prepared also on carbon nanotube templates.[7] *Ab-initio* calculations showed that, irrespective of their chirality, NbS_2 nanotubes are metallic with a large density of states in the Fermi level.[8]

The various Nb–S phases were first investigated by Jellinek *et al.*[9,10] Two polymorphs of the layered disulfide were identified: the rhombohedral-3*R* (*R*3*m*) polytype with a unit cell consisting of three NbS_2 slabs which is formed when the elements are heated below 800 °C, and the hexagonal-2*H* ($P6_3/mmc$) polymorph with a unit cell consisting of two NbS_2 slabs, is obtained above 850 °C. Nonstoichiometric $3R\text{-}Nb_{1+x}S_2$ compounds were also found.[10] Further studies showed that the 3*R* polytype exists for at least $0 < x < 0.18$, while the 2*H* polytype is stable only for small deviations from stoichiometry.[11] Both phases exhibit metallic behavior, and the 2*H*-phase shows even superconductivity below 6.23 K.[11]

The synthesis of TiS_2 by the reaction of $TiCl_4$ with H_2S has been known for a long time.[12] Rose[13] reacted a mixture of $NbCl_5$ and $TaCl_5$ (''Chlorpelop'') with H_2S converting it to the sulfide. More recently, thio-sol–gel reactions have been used for the synthesis of TiS_2 and NbS_2 powders.[14] Interestingly, submicron spherical particles of the two compounds were found after annealing at relatively mild temperatures (550 °C). At higher annealing temperatures the spherical particles gradually converted into platelets. Unfortunately, analysis with transmission electron microscopy, which could shed some light on the structure of the particles and their morphological transformations, was not reported in this study. Low temperature metathetical synthesis of various MS_2 compounds, including the synthesis of NbS_2 using $NbCl_5$ and Li_2S in tetrahydrofuran solution, was demonstrated.[15]

In the present report an alternative approach has been adopted for the synthesis of NbS_2 onions (*IF*), by reacting $NbCl_5$ with H_2S and subsequent annealing. The annealing process was followed using transmission electron microscopy, which revealed the gradual removal of defects from the nested nanostructure until a highly crystalline nanoparticle is obtained.

Experimental

The synthesis used in the present paper bears some similarities to the one reported in ref. 7 where NbS_2 nanotubes were produced on carbon nanotube templates using $NbCl_4$ precursor. However, in the present work the pentachloride was used and no template was employed. Consequently nanoparticles with different morphologies were obtained. Fig. 1 shows the reactor used for the present synthesis. $NbCl_5$ (b.p. 254 °C) was evaporated by preheating a container with 0.5 g of the compound to 200 °C. The $NbCl_5$ vapor was mixed with N_2 gas (flow rate *ca.* 100 ml min^{-1}) and led to the main reactor (maintained at a temperature of about 400 °C). A gas mixture of H_2S and forming gas (5% H_2; 95% N_2) was fed into the main reactor, too. It was allowed to react with the preheated $NbCl_5$ vapor according to the reaction:

$$(1 + x)\ NbCl_5\ (g) + (0.5 + 2.5x)\ H_2 + 2\ H_2S \rightarrow Nb_{1+x}S_2\ (s) + (5 + 5x)\ HCl\ (g) \quad (1)$$

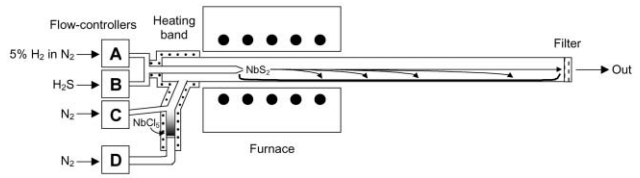

Fig. 1 Schematic drawing of the reactor used for the synthesis of the NbS_2 nanoparticles. $NbCl_5$ powder is placed on a quartz frit and heated to 200 °C. N_2 gas (flow-controller D) takes the vapor up. It is diluted with N_2 from flow-controller C. In the main reactor (furnace at 400 °C) the $NbCl_5$–N_2 gas mixture meets a mixture of forming gas (5% H_2, 95% N_2; flow-controller A) and H_2S (flow-controller B) coming out of a nozzle. There a chemical reaction occurs forming $Nb_{1+x}S_2$ and HCl. The fine $Nb_{1+x}S_2$ powder precipitates on the boat and the filter. The gases are taken out to washing bottles.

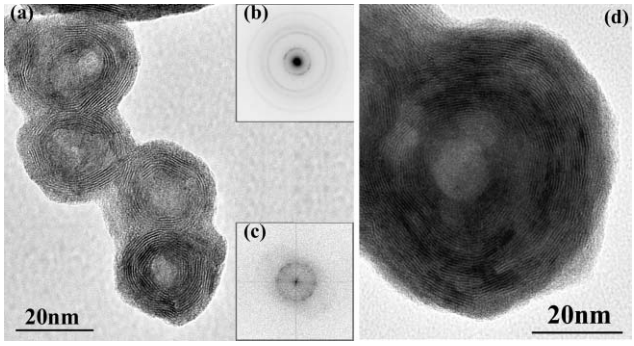

Fig. 2 TEM micrograph of a few NbS_x nanoparticles with a non-perfect *IF* structure after the reaction. (a) Image of a group of a few *IF*-NbS_2 nanoparticles; (b) SAED of a group of such nanoparticles; (c) FFT of one of the nanoparticles; (d) large *IF*-NbS_2 nanoparticle obtained in the same reaction.

In fact, the value of x varied between $0 < x < 1$. Stable intermediates $NbSCl_3$ and NbS_2Cl_2, which decompose into NbS_2 upon heating, were identified.[16] Premature reaction of the $NbCl_5$ vapor and H_2S gas would generally lead to a product with a poorly defined composition. To allow the $NbCl_5$ vapor and H_2S gas to heat up before reaction and produce distinct chemical phases, the two gases were made to mix with each other close to the middle of the reactor (see Fig. 1).

The reaction products were collected on a filter inserted at the colder end (downstream) of the reactor and analyzed using transmission electron microscopy (TEM; 120 keV); X-ray energy dispersive analysis (EDS); and selected area electron diffraction (SAED). A scanning electron microscope (SEM) equipped with a EDS detector was also used for the analysis of the product.

Results

Table 1 summarizes the results of two out of many experiments, in which the synthesis of the NbS_2 nanoparticles according to Eqn. 1 was attempted. Fig. 2 shows TEM micrographs of a representative product from sample #1. Nanoparticles of close to spherical shape and closed nature (*IF*-NbS_2) are obtained. The nanoparticles are not fully detached from each other and they are also not perfectly crystalline containing numerous edge dislocations. Two kinds of *IF* nanoparticles are obtained in this synthesis. One family consists of relatively small nanoparticles (<30 nm), which is only partially crystallized (Fig. 2a–c). The other kind of nanoparticles (Fig. 2d) is larger (50 nm) and also more crystallized than the former kind. However, these nanoparticles contain numerous edge dislocations, and consequently although the NbS_2 layers are curved they are not fully closed. In fact more detailed analysis of the nanoparticles belonging to the first family in Fig. 2a reveals that they contain four distinct zones. The core of the nanoparticles does not seem to be hollow. Rather it consists of an amorphous (NbS_x) material. Further out there are a few folded but not fully closed NbS_2 layers. They appear to have started the crystallization process, but the short residence time in the furnace (<10 s) did not allow them to complete this process. On top of these layers, almost fully crystalline and closed NbS_2 layers can be discerned. These layers, however, intersperse with the NbS_2 layers of the adjacent nanoparticles making this whole agglomerate inseparable, even after a short ultrasonic treatment. Furthermore, a continuous top layer of amorphous material enfolds the nanoparticles and "glues" them together into an agglomerated superstructure. The nature of this amorphous coating does not seem to be different from the one in the nanoparticles' core. In general, the nanoparticles exhibit non-perfect crystallinity with numerous defects and some amorphous material interspersed with the crystalline NbS_2 layers. The composition of the nanoparticles cannot be easily verified. EDS analysis reveals that only Nb and S are present in the nanoparticles with an Nb : S ratio of approximately 1 : 1 for samples of this kind. The excess niobium in this sample is probably present in the amorphous core and the outer amorphous envelope of the nanoparticles. Note, however, that excess Nb intercalation between the NbS_2 layers[17] is not unlikely in this case. When the source temperature was reduced to 180 °C (sample #2 of Table 1), appreciably smaller (<20 nm) nanoparticles with quasi-spherical morphology and a higher degree of crystallinity were obtained.

As mentioned above NbS_2 may appear in two polytypes, hexagonal-2*H* ($P6_3/mmc$) and trigonal-3*R* ($R3m$). Due to the close similarity in the *d* values of the two structures it is rather difficult to assign the polytype of the particles from their electron diffraction ring pattern, however they seem to be closer to the trigonal 3*R* form. Analysis of the SAED pattern, obtained from a zone containing a few nanoparticles (Fig. 2b), shows that the average (00*l*) interlayer spacing is 6.15 Å. Fast Fourier transform (FFT) from images of individual particles, in the non-annealed sample (Fig. 2c), shows a rather diffuse ring, corresponding to interlayer spacing in the range 5.9–6.35 Å for the small (20–40 nm) particles and 6.2 Å for the larger (60–80 nm) ones.

In order to improve the crystallinity of the nanoparticles, the samples collected after the synthesis were annealed at 550 °C for various periods of times under H_2S and H_2 atmosphere. Table 2 shows the experimental parameters of the annealing of

Table 1 Experimental parameters used for the synthesis of the hollow NbS_x nanospheres—step I. On the way through the furnace (15 to 20 seconds) $NbCl_5$ vapor reacts with H_2S and H_2 gas yielding amorphous but pre-structured nanoballs. The samples were collected from the filter at the end of the tube, which remained at room temperature throughout the reaction. The lower temperature at the heating band provided a lower concentration of $NbCl_5$ vapor. The nanoballs of sample #2 are smaller compared to sample #1

			Flow-controllers			
Sample #	T($NbCl_5$ source)/°C	T(furnace)/°C	A: 5% H_2 (in N_2)/ml min^{-1}	B: H_2S/ ml min^{-1}	C: N_2 (diluting)/ ml min^{-1}	D: N_2 (carrier)/ ml min^{-1}
1	200	400	28	6	90	14
2	180	400	28	6	90	14

Table 2 Annealing of pre-structured nanoballs—step II. The nanoballs of sample #1 were annealed at 550 °C under a flow of a gas mixture of 5% H_2 (in N_2) and H_2S for various times. The crystalline structure became more and more ordered yielding hollow core *IF*-NbS_2 onion-like particles

		Flow-controllers		
Sample #	*T*(furnace)/ °C	A: 5% H_2 (N_2)/ ml min^{-1}	B: H_2S/ ml min^{-1}	Annealing time/ min
3	550	15	3	10
4	550	15	3	30
5	550	15	3	60
6	550	15	3	130
7	550	15	3	225

sample #1. Fig. 3a shows a TEM image of a typical group of nanoparticles after 130 minutes of annealing. Fig. 3b shows an expanded view of one of the *IF*-NbS_2 nanoparticles. The annealed samples exhibit a few salient differences with respect to the non-annealed samples. First the amorphous halo around the nanoparticles has now partially disappeared and converted into fully crystalline NbS_2 layers. These layers further enfold the already existing closed NbS_2 layers, and also interconnect neighboring nanoparticles. Equally important is the fact that the amorphous layer in the center of the annealed nanoparticles has partially crystallized, too, and formed closed faceted NbS_2 layers, leaving an empty core in the center of the nanoparticle. EDS analysis of the samples annealed for 130 minutes shows that the Nb : S ratio approaches 1 : 2, *i.e.* $Nb_{1+x}S_2$. Samples annealed for less than 2 h presented an intermediate case between the fully annealed and the non-annealed samples, while samples annealed for longer periods of times exhibited a gradual coarsening, which stems from the close proximity of the agglomerated nanoparticles. Also, the density of edge dislocations is considerably reduced after the annealing and the nanoparticles are much more faceted. The inner hollow core of the nanoparticles exhibits distinct angles, most typically 90°. In several cases, the inner core seems to have formed an octahedron. Polyhedra of MoS_2 with octahedral structures have been suggested[2] and later reported.[18] They consist of six MoS_2 squares in the apices of the octahedra, and are believed to be the most stable form of MoS_2 nanoclusters. In contrast with MoS_2, in which the Mo atom is coordinated to the sulfur atoms in a trigonal prismatic arrangement, the Nb is coordinated to the S atoms in an octahedral arrangement. It is thought that the latter kind of coordination would prefer the octahedral polyhedra. However, more work is necessary to validate this concept.

Comparison of the electron diffraction patterns of the non-annealed particles and the annealed samples shows a shift in the

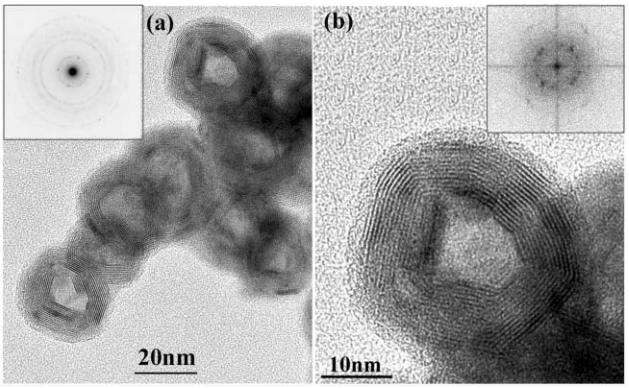

Fig. 3 TEM micrographs of the annealed *IF*-NbS_2 nanoparticles: (a) a group of such nanoparticles and their SAED in the inset; (b) higher magnification of one of the nanoparticles showing the closed nature of the layers and FFT of the nanoparticle in the inset.

Table 3 Experimental parameters for the synthesis of Nb_2O_3 nanoflowers and sea urchin-like particles (samples #8 and #9), and also NbS_2 nanowhiskers (sample #10) with a modified apparatus

			Flow-controllers	
Sample #	*T*($NbCl_5$ source)/ °C	*T*(furnace)/ °C	A: 5% H_2 (N_2)/ ml min^{-1}	B: H_2S/ ml min^{-1}
8	225	900	100	4.0
9	225	1050	100	4.0
10	225	400	25	5.0

(00*l*) layer spacing from 6.15 to 5.9 Å upon annealing (inset of Fig. 3a). FFT of images from a single nanoparticle of the annealed samples (inset of Fig. 3b) results in a pattern comprising sharp spots (layer spacing of 5.9 Å), including high order ones, which are indicative of a more ordered structure.

In a related synthetic approach amorphous and crystalline NbO_xS_y nanofibers were obtained. In this reactor the $NbCl_5$ vapor was mixed with forming gas (5% H_2; 95% N_2 at 100 ml min^{-1}) rather than with pure N_2 gas, before being swept to the main reactor. Table 3 shows the experimental conditions used for this series of experiments.

Figs. 4 and 5 show TEM micrographs of fibrillar nanostructures from samples #8 and #9. Fig. 6 shows SEM images of the same nanofibers (#8). The nanofibers seem to emanate from one center and grow in all directions thus forming 3-D hemispherical nanoflower patterns. The nanostructures were amorphous and did not produce any SAED pattern. EDS

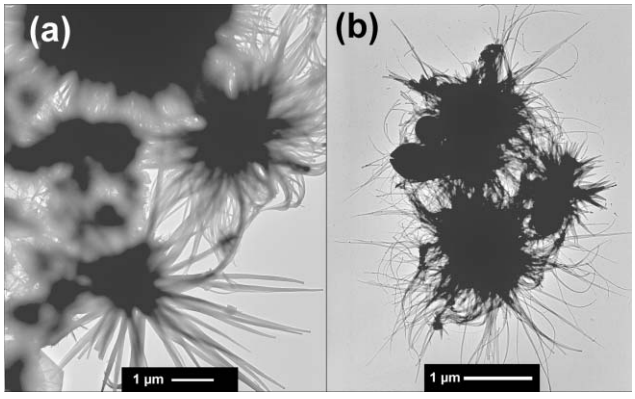

Fig. 4 TEM micrographs of amorphous NbO_xS_y nanoflowers from sample #8 (synthesized at 900 °C). (a) Three particles stuck to each other by their intertwining thin needles; (b) longer and thicker needles obviously emanating from one center of nucleation.

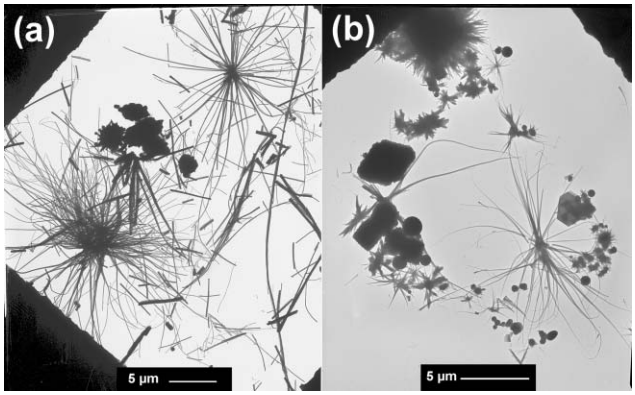

Fig. 5 TEM micrographs of amorphous NbO_xS_y nanoflowers from sample #9 (synthesized at 1050 °C). (a) The needles are much longer compared to Fig. 4; (b) the sample is not homogenous concerning the particle shape, nanoflowers with long needles are mixed with some sphere-like particles; particles with a bigger center exhibit shorter needles. This points to a root growth mechanism.

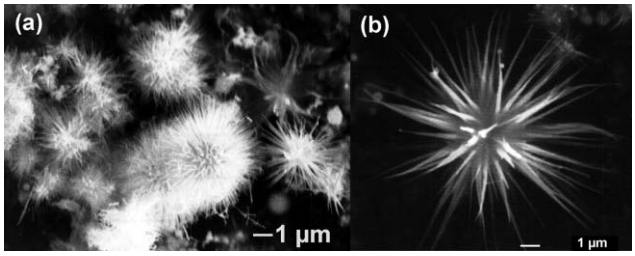

Fig. 6 SEM micrographs of nanoflowers from sample #8, showing two typical morphologies: (a) sea urchin-like shapes; (b) star-like morphology, which seems to be a later level in the growth process, since the needles are longer and the sphere-like center is smaller.

analysis of the products was carried out. Short incipient nanofibers were composed mostly of Nb with little sulfur and oxygen. The composition of the developed (long) nanofibers varied between $NbO_{1.6}S_{0.1}$ and $NbO_{1.7}S_{0.2}$. This composition can be related on the lower (oxide) end to Nb_2O_3, which is a stable, but not so common oxide phase of niobium.[19] On the higher (O + S) end this composition can be associated with the much more common compound NbO_2. Similar patterns were previously obtained for SiO_x nanoflowers by firing SiC powder over a Co catalyst.[20] A similar growth pattern was observed also for carbon nanotubes grown from a central Co particle.[21] However, in the present work, no metallic catalyst is used *a priori*. Attempts to convert these nanofibers into NbS_2 nanotubes or crystallize them by annealing under different atmospheres and temperatures were unsuccessful. When the synthesis was carried out at lower temperatures (400 °C) and a slower flow rate of the forming gas (25 ml min^{-1}), crystalline NbS_2 nanofibers were obtained (see Fig. 7). Comparing the images from samples #8 and #9, one can see that at 900 °C (sample #8, Fig. 4) the needles have a length of less than 3 μm and the center of nucleation has a diameter of about 1 μm (black area in the TEM image). However at 1050 °C (sample #9, Fig. 5) much longer fibers can be observed (>10 μm) without a black area at the center; particles with shorter needles (top of Fig. 5b) similar to sample #8 are also found here. It looks like the material in the center serves as a supply for the needle growth (root growth). At higher temperatures the growth reaction is faster, thus—after this supply is consumed—the needles are longer.

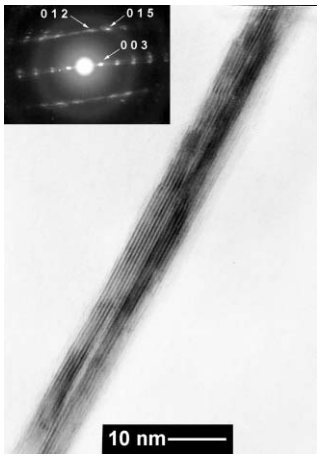

Fig. 7 TEM micrograph of a crystalline NbS_2 nanowhisker from sample #10. The inset displays the SAED pattern of this nanowhisker, and reveals a layer distance of 5.99 Å in accordance with the distance of the lines measured from the image (5.9 Å). Investigation of the other reflections points to the 3*R* rather than the 2*H* phase, but a mixture of both cannot be excluded. Indices for the 3*R* phase are given in the inset.

Discussion

A rough estimate of the free energy change involved in Eqn. 1, using the data of ref. 22, shows that, while this reaction is almost balanced at room temperature, it becomes highly exothermic (<-150 KJ mol^{-1}) at 400 °C. In analogy to metathesis reactions,[23] which are highly exothermic at elevated temperatures, ignition of the reaction leads to a very rapid and sometimes explosive progression. The rapid reaction leads to a high degree of supersaturation of the vapor, and hence to a fast nucleation. The fast kinetics of the reaction together with the short residence time in the oven does not permit the crystallites to grow to a macroscopic size and consequently NbS_2 nanocrystallites with *IF* structure are formed.

It is very likely that amorphous NbS_x nanoparticles are formed in the vapor. The crystallization and the formation of the incipient *IF* structures occur before these nanoparticles agglomerate. Since the residence time of the nanoclusters within the hot zone of the reactor is not longer than a few seconds, the reaction of the amorphous NbS_x nanoparticles with H_2S and the crystallization of incipient *IF*-NbS_2 cannot be completed. Therefore, the nanostructures are heavily dislocated and the NbS_2 layers are not always fully closed. Further annealing of the product in H_2S and H_2 gases is necessary in order to produce a more perfectly crystalline phase. The annealing temperature cannot be too high, since otherwise coarsening of the agglomerated nanoparticles is unavoidable. Following 2–4 h annealing at 550 °C the nanoparticles become highly crystalline, but also faceted. Furthermore, the amorphous matter in the center of the nanoparticle has reacted with sulfur, forming new closed NbS_2 layers. The innermost NbS_2 layers, close to the now hollow core of the nanoparticles, become highly faceted with very sharp angles. In future work, synthesis in a fluidized bed reactor will be attempted. In this reactor the nanoparticles are kept aloft in the gas phase and do not interact with each other. This will allow annealing at higher temperatures without the danger of coarsening and loss of the *IF* structure.

A continuum theoretical analysis of the morphology of closed cage structures was undertaken.[24] This analysis suggests that closed cage structures of relatively large radius of curvature (>10 nm) and thin walls will bend uniformly and form quasi-spherical nanostructures. However, when the dimensions of the nanostructures go below a critical size the bending energy becomes excessively high, and point defects (grain boundaries) become energetically more favorable. Consequently a phase transition into a polyhedral structure is predicted in this case. This idea was validated by careful inspection of the growth of *IF*-WS_2 nanoparticles from tungsten oxide nanoparticles.[25] Here, the oxide to sulfide reaction proceeds from the outer surface of the oxide nanoparticle to the inner core. Hence the diameter of the first few closed WS_2 layers is large and they adopt a quasi-spherical shape. However, when the reaction proceeds, the oxide core is slowly consumed by the sulfide layers, which form closed WS_2 layers with an ever-smaller diameter. At a certain point faceted WS_2 polyhedral *IF* structures appear, which confirms the above theory. In the present case, the annealed samples are typified by having a thicker NbS_2 shell, *i.e.* a larger number of NbS_2 layers, than the non-annealed samples. Furthermore, the density of edge dislocations decreased after the annealing, making the faceting a more likely mechanism for the strain relief in the closed cage structures. These developments explain the transformation of the synthesized quasi-spherical NbS_2 nanoparticles into faceted polyhedra, after the annealing. Obviously, more work is needed to evaluate the most stable arrangements of NbS_2 polyhedral structures.

The formation of amorphous nanoflowers having a composition very close to Nb_2O_3 is quite unusual. In contrast to the previous works, which discussed the growth mechanism of

nanoflowers of SiO_x[19] and carbon nanotubes,[20] there is no apparent catalyst in the present process. Two questions arise in this respect. What is the growth mechanism of these nanofibers and what is the catalyst that promotes such growth (if there is any)? Two well-established growth mechanisms for whiskers are the so-called vapor liquid solid (VLS) mechanism,[26] and the Bravais–Friedel–Donnay–Harker model.[27] In the first mechanism, the vapor reacts with a liquid droplet at the top of the growing nanowhisker. In order to maintain the degree of supersaturation, the liquid droplet deposits a solid whisker, which grows behind inaccessibly until the vapor pressure in the gas or the growth temperature decreases. The second mechanism pertains to solids with an asymmetric unit cell. The preferred crystal direction for the nanowhisker growth is along the direction where the lattice parameter is the smallest, *i.e.* the highest density of surface bonds is available for the vapor to interact with. Analysis of the data suggests that the nanofibers growth can be described as a root growth mechanism, where a common reservoir of material exists in the epicenter. A volatile phase condenses on this reservoir, leading to its supersaturation with respect to NbO_x, which promotes the nanofiber growth. More work is needed in order to clarify these points and use this growth mode in order to obtain NbS_2 nanotubes.

Acknowledgement

This research is supported by the German-Israeli Foundation (GIF) and the G. Schmidt Minerva Center for Supramolecular Chemistry.

References

1 R. Tenne, L. Margulis, M. Genut and G. Hodes, *Nature*, 1992, **360**, 444.
2 L. Margulis, G. Salitra, R. Tenne and M. Talianker, *Nature*, 1993, **365**, 113.
3 N. G. Chopra, J. Luyken, K. Cherry, V. H. Crespi, M. L. Cohen, S. G. Louie and A. Zettl, *Science*, 1995, **269**, 966.
4 (*a*) Y. Q. Zhu, W. K. Hsu, S. Firth, M. Terrones, R. J. H. Clark, H. W. Kroto and D. R. M. Walton, *Chem. Phys. Lett.*, 2001, **342**, 15; (*b*) Y. Q. Zhu, W. K. Hsu, M. Terrones, S. Firth, N. Grobert, R. J. H. Clark, H. W. Kroto and D. R. M. Walton, *Chem. Commun.*, 2001, 121.
5 M. Nath and C. N. R. Rao, *J. Am. Chem. Soc.*, 2001, **123**, 4841.
6 R. Tenne, *Prog. Inorg. Chem.*, 2001, **50**, 269.
7 Y. Q. Zhu, W. K. Hsu, H. W. Kroto and D. R. M. Walton, *Chem. Commun.*, 2001, 2184.
8 G. Seifert, H. Terrones, M. Terrones and T. Frauenheim, *Solid State Commun.*, 2000, **115**, 635.
9 F. Jellinek, G. Brauer and H. Müller, *Nature*, 1960, **185**, 376.
10 F. Kadijk and F. Jellinek, *J. Less-Common Met.*, 1969, **19**, 421.
11 W. G. Fisher and M. J. Sienko, *Inorg. Chem.*, 1980, **19**, 39.
12 V. W. Biltz, P. Ehrlich and K. Meisel, *Z. Anorg. Allg. Chem.*, 1937, **234**, 97.
13 H. Rose, *Ann. Phys. Chem.*, 1846, **69**, 115.
14 M. A. Sriram and P. N. Kumta, *J. Mater. Chem.*, 1998, **8**, 2441.
15 R. R. Chianelli and M. B. Dines, *Inorg. Chem.*, 1978, **17**, 2758.
16 H. Schäfer and W. Beckmann, *Z. Anorg. Allg. Chem.*, 1966, **347**, 225.
17 (*a*) M. Remskar and Z. Skraba, *Surf. Sci.*, 1996, **365**, L652; (*b*) C. Zhou and L. W. Hobbs, *Mater. Res. Soc. Symp. Proc.*, 1993, **295**, 195.
18 P. A. Parilla, A. C. Dillon, K. M. Jones, G. Riker, D. L. Schulz, D. S. Ginley and M. J. Heben, *Nature*, 1999, **397**, 114.
19 *CRC Handbook of Chemical Physics*, 69th edn., CRC Press, Boca Raton, FL, 1988–1989, p. B-111.
20 Y. Q. Zhu, W. K. Hsu, M. Terrones, N. Grobert, W. B. Hu, J. P. Hare, H. W. Kroto, D. R. M. Walton and H. Terrones, *Chem. Mater.*, 1999, **11**, 2709.
21 S. Subramoney, R. S. Ruoff, D. C. Lorents and R. Malhorta, *Nature*, 1993, **366**, 637.
22 *Standard Potentials in Aqueous Solution*, eds. A. J. Bard, R. Parsons and J. Jordan, Marcel Dekker, Inc., New York, 1985.
23 E. G. Gillan and R. B. Kaner, *Chem. Mater.*, 1996, **8**, 333.
24 D. J. Srolovitz, S. A. Safran, M. Homyonfer and R. Tenne, *Phys. Rev. Lett.*, 1995, **74**, 1778.
25 Y. Feldman, G. L. Frey, M. Homyonfer, V. Lyakhovitskaya, L. Margulis, H. Cohen, G. Hodes, J. L. Hutchison and R. Tenne, *J. Am. Chem. Soc.*, 1996, **118**, 5362.
26 R. S. Wagner and W. C. Ellis, *Appl. Phys. Lett.*, 1964, **4**, 89.
27 (*a*) J. D. Donnay and D. Harker, *Am. Mineral.*, 1937, **22**, 446; (*b*) A. S. Myerson, in *Molecular Modeling Applications in Crystallization*, ed. A. S. Myerson, Cambridge University Press, Cambridge, 1999.